

Analysis of Fractures and Microstructures on Different Injection Speeds in High-Pressure Die-Casting Magnesium Alloy

M D Ibrahim^{1*}, J Jendia¹, Y Kashiwabara³, L B Roslan¹, H Watanabe², Y Sunami³

¹Department of Mechanical and Manufacturing Engineering, Faculty of Engineering, Universiti Malaysia Sarawak, Jalan Datuk Mohammad Musa, 94300 Kota Samarahan, Sarawak, MALAYSIA

²Kyokuto Die-Casting Co., Ltd., 57 Mukohara, Yamakita, Ashigarakami, Kanagawa, 258-0111, JAPAN

³Department of Mechanical Systems Engineering, Tokai University, 4-1-1 Kitakaname, Hiratsuka, Kanagawa, 259-1292, JAPAN

*Corresponding Author

DOI: <https://doi.org/10.30880/ijie.2023.15.05.013>

Received 9 June 2023; Accepted 18 June 2023; Available online 19 October 2023

Abstract: In this study, to clarify the unknown physical properties of the Mg-Al-Th-RE alloy, the relationship between the injection conditions and the internal porosities, and the mechanical properties exerted by the solidification microstructure was investigated. The obtained cast samples were investigated using X-ray CT internal measurements, tensile tests, Vickers hardness tests, and solidification microstructure observations. The tensile strength and the elongation at the injection speed of 5.0 m/s were higher than at 2.0 m/s. The number of porosities affected the tensile strength and the elongation even at the same fracture position. In addition, it was confirmed that segregation affected the destruction smaller the porosity size and the greater the variability of porosity. As the injection speed increased, the amount of heat transferred between the molten metal and the wall surface also increased, resulting in quick freezing and solidification. The tensile strength increased at the injection speed of 5.0 m/s because the interface between the scattered primary crystals and eutectic systems was narrow. On the other hand, at the injection speed of 2.0 m/s, the tensile strength decreased because the molten metal was delayed in solidification and dendrite growth became remarkable.

Keywords: Tensile strength, elongation, injection speed, porosity

1. Introduction

High-Pressure Die Casting (HPDC) is a technology that is indispensable to produce magnesium parts. HPDC is a casting method that injects molten metal into a mold at high speed and high pressure, thereby shortening the manufacturing cycle as much as possible. For this reason, die casting has been established as a system capable of mass-producing products with excellent casting surfaces in a short time. However, characteristic porosities such as porosity and inclusion of solidified fragments occur in die-cast products. In particular, the cavities caused by air entrainment and solidification shrinkage cause not only deterioration of mechanical properties but also leakage of pressure-resistant members. Therefore, there is a need to elucidate the mechanism of porosity generation and optimization of the injection speed has been performed with CFD [1], [2], [3]. Research related to quantitative measurements is also being

performed [4], [5]. These studies have been actively conducted on aluminum alloys and zinc alloys. Although, research and developments on magnesium alloys have not progressed because of material features such as flammability and poor castability. Magnesium alloys are generally difficult to cast because of the ignition, low specific heat, easy solidification, and poor fluidity. Heat-resistant and flame-retardant magnesium alloys with improved properties have been actively used and have been applied to automotive parts as practical materials [6], [7], [8]. Among them, Mg-Al-Th-RE alloy is a magnesium alloy with improved flame retardancy by calcium (Ca) and heat resistance by Thorium (Th) and rare-earth (RE) elements, and with excellent fluidity to which aluminum (Al) is added at about 8% or more. It is expected to be used for products with complicated shapes that make filling the molten metal uniformly difficult.

However, Mg-Al-Th-RE alloy internal microstructures and mechanical properties have not been elucidated for those cast in die-casting processes. Die-casting magnesium alloys generally have eutectic microstructures composed of primary and eutectic phases crystallized from a liquid phase. According to Mondal et al., the microstructures of magnesium alloy MRI153M are primary phase α -Mg and eutectic $Mg_{17}Al_{12}$ and $(Mg, Al)_2Ca$ phases, and the number of $(Mg, Al)_2Ca$ is related to creep behavior [9]. Sun et al. examined the effect of casting thickness on the tensile properties of AZ91 magnesium alloy. The high tensile properties were attributed to the low porosity level, fine dendrite microstructure, high eutectic content, and thick skin due to decreasing thickness [10]. This literature shows that it is necessary to know the correlation between the solidification microstructure and the material strength and to find conditions that can maximize its physical properties.

In this study, the relationship between the injection conditions and the internal porosities, and the mechanical properties exerted by the solidification microstructure were investigated to clarify the unknown physical properties of the Mg-Al-Th-RE alloy. The obtained cast samples were investigated using X-ray CT internal measurements, tensile tests, and solidification microstructure observations.

2. Experimental Method

2.1 Simulation Method

Table 1 shows the chemical composition of the Mg-Al-Th-RE alloy. The Mg-Al-Th-RE alloy is flame-retardant. The flame retardancy by Ca and strontium (Sr) and the heat resistance by Th and Lanthanum (La) of rare earth have been improved. Figure 1 shows the analysis model used in this paper. The cavity size is 200 mm in height, 100 mm in width, and 4, 8, 12, and 16 mm in thickness. The different thicknesses will help to explain casting properties followed by each thickness of die-casting products. The runner was a typical T-shape, and the overflow was set on the side of 12 mm and 16 mm parts, which were the final filled positions. The physical properties of the Mg-Al-Th-RE alloy were obtained by the material properties calculation software JMatPro. This software calculates thermodynamic properties from the chemical composition of an alloy. The mold-filling process was simulated with the casting simulation software JSCAST. The basic equations were the continuity equation, the Navier-Stokes equation, and the energy equation. The simulation methods were a three-dimensional numerical model of the single-phase flow of liquid phase based on the direct finite difference method and the Volume of Fluid (VOF) method. Table 2 shows the analysis conditions. The thermophysical properties of the Mg-Al-Th-RE alloy determined by the JMatPro were set as the material parameters. The die material was the SKD61 for die steel. The meshing properties were based on orthogonal elements of 1.0 mm where Tetra-meshes were applied to the model surface. The injection conditions were the two-stage injection with the first injection speed v_1 of 0.3 m/s and second speed v_2 of 2.0 and 5.0 m/s. When the model is filled at 39.6%, the injection speed is switched to high speed. The calculation was finished at the filling rate of 99% and is considered as converged. The vent pressure was the atmospheric pressure and the flow was stopped if the internal pressure of the air in the mold exceeded 20 MPa. The gate thickness was 6.0 mm from the flat side. It was determined due to relatively easy cutting on actual casting.

Table 1 - Chemical composition of the Mg-Al-Th-RE alloy (mass %)

Al	Th	Ca	Sr	Ce	Mn	La	Pr	Si	Y	Mg
8.51	2.26	>0.42	0.22	0.14	0.11	0.079	0.045	0.027	0.020	Bal.

2.2 Casting Method

The step-type test pieces were manufactured by HTPC using a 350-ton cold chamber die-casting machine (Ds-350EX, Toyo Machinery & Metal Co., Ltd.). Figure 2 shows a schematic die-casting system. Table 3 shows the casting conditions. The gate thickness was 6.0 mm. The second injection speed was set to 2.0 m/s and 5.0 m/s. Ten specimens were prepared under the conditions and the mechanical property measurements and were performed on four randomly selected samples. A tensile test specimen was 20 mm wide, 4 mm thick, and 25 mm gage length. As shown in Figure 3, the test specimen was 4 mm thickness of test piece, using water jet cutting in as-cast. Tensile tests were carried out with a 1 mm/min crosshead rate using a universal testing machine (Shimadzu Corporation, AG-100 kN X plus). X-ray CT (Nikon Instech, XTH225) was used for internal porosity measurement. The X-ray CT shows in Figure 4. Four specimens were set on the jig not to move them to obtain proper X-ray tomography. The jig was made of a Styrofoam

stage and an acrylic base plate. Styrofoam spacers used to simplify the analysis process were inserted between the specimens. The four fractured specimens were overlapped to suppress the variation in the transmittance with angles. This is because a single sample has a noticeable difference in the amount of transmission due to the variance between the width of 20 mm and the thickness of 4 mm, making it difficult to match the overall resolution. The object to be photographed was regarded as a prism with a top surface of 20 mm x 25 mm including the spacer, and only the parallel part with a width of 20 mm was measured. At this time of measurement, the minimum detectable porosity diameter was approximately about 0.06 mm. The CT reconstruction was performed using CT Pro (Nikon). The beam hardening was applied to the photographed image because metal artifacts were noticeable. CT analysis software (Volume Graphics, VG Studio MAX 3.1) was used for porosity analysis. The boundary between the object and surrounding air was determined using the center gradation between the peaks of the color histogram of the reconstructed CT data. If the void detection is performed using the algorithm, the difficult void to confirm as porosity is detected. In this paper, the void was detected through the threshold analysis method. The threshold analysis method qualitatively detects the void using the threshold value of the grayscale to be regarded as porosity. This method can reduce a low accuracy void. For the microstructure observation, the observation surface was sanded and buffed in the order of # 150, # 500, # 800, and # 2000, and finished with a mirror surface. Next, a nitric acid concentration of 5% with metal was etched for 30 seconds. The obtained corrosion surface was observed with an industrial microscope (Nikon, ECLIPSE L150).

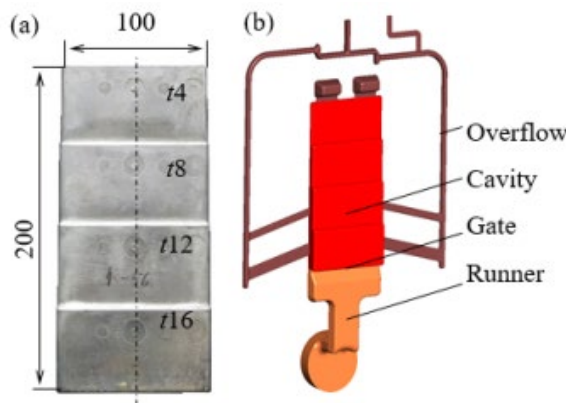


Fig. 1 - Schematic diagram of the steps-type test piece (a) front view with dimensions of the test piece; (b) internal geometry of the metal

Table 2 - Simulation conditions

Fluid		Mg alloy
Mold		SKD61
Injection speed	First v_1 [m/s]	0.3
	Second v_2 [m/s]	2.0, 5.0
Casting pressure P [MPa]		70
Temperature T [K]		953
Kinematic viscosity ν [m ² /s]		1.0×10^{-6}
Critical pressure P_c [MPa]		20
The thickness of gate t_g [mm]		6.0
Mesh size l [mm]		1.0

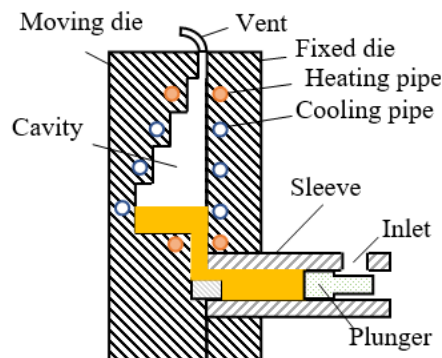


Fig. 2 - Schematic diagram of the die-casting machine

Table 3 - Casting conditions

Method		HPDC
Machine		Ds350EX Toyo Machinery & Metal Co., Ltd.
Injection speed	Slow v_1 [m/s]	0.3
	Fast v_2 [m/s]	2.0, 5.0
Casting pressure P_c [MPa]		70
Pouring temperature T_p [K]		953
Die temperature T_d [K]		423
Gate thickness t_g [mm]		6.0
Number N		10

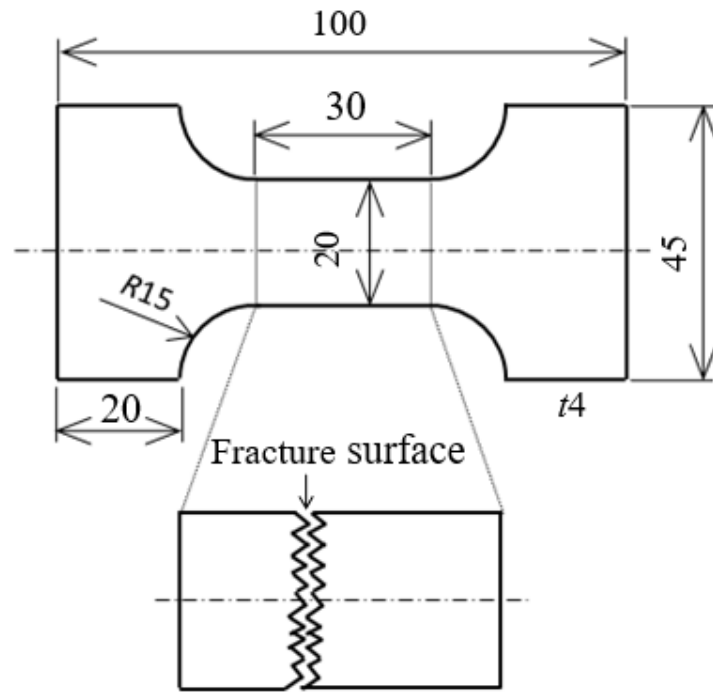
3. Results and Discussions

3.1 Destruction Type and Stress-Strain Curve

Figure 5 shows that the destruction type for the plate thickness of 4 mm at the injection speed of 2.0 m/s. These figures show the X-ray CT results of the reduced section of the tensile test specimens. And figure 6 shows the stress-strain curve for the plate thickness of 4 mm at the injection speed of 2.0 m/s. Sample A has a bow-like fracture that is severely undulating between a group of porosities with a length of more than 1 mm and a group of porosities with a length of 0.3 mm or less. The large porosities for the left side of the fracture surface were due to a hot spot and the little porosities for the right side of the fracture surface were due to early solidification. In the temperature distribution of the simulation shown in Figure 7, a steep temperature gradient was confirmed in the fracture surface of sample A. In the liquid phase and the solid phase coexistence region with a high-temperature gradient, the remaining liquid phase on the left side moved to the right side due to the little liquid phase in the dendrite gap then many porosities were generated on the left side. Therefore, the tensile strength and elongation were significantly lower than those of other samples because the cracks were generated from segregation. Sample B was the flat fracture surface due to a brittle fracture. The porosities were sparsely distributed, and their segregation was low. However, in the temperature distribution of the simulation, it was highly possible that the fracture occurred at a steep temperature gradient position and segregation occurred. Therefore, it was considered that the tensile strength was as low as 180 MPa. Sample C broke at the same position as sample A and showed a fracture surface that was a combination of undulations and flatness. The porosities were relatively distributed near the fracture surface. From the simulation results, segregation was likely to occur in this case, and the undulating fracture was considered to be greatly affected by segregation. The stress and the elongation showed median values of samples A and B showed the effects of both segregation and brittle fracture. Although the porosities of sample D were sparsely distributed like sample B, it was destroyed in the fillet instead of the reduced section.

Figure 8 shows that the destruction type for the plate thickness of 4 mm at the injection speed of 5.0 m/s. Figure 9 shows that the stress-strain curve for the plate thickness of 4 mm at the injection speed of 5.0 m/s. Samples E and F had almost the same fracture position and a flat fracture surface. However, the tensile strength and the elongation were higher in sample F which had a smaller porosity size and quantity. The porosities with a diameter of 0.5 mm or less were widely distributed in sample E, whereas in sample F, porosities with a diameter of 0.3 mm or less were distributed from the upper left to the lower right. It was confirmed that the number of porosities affected the tensile strength and the elongation even at the same fracture position. In addition, it was confirmed that the tensile strength and the elongation at the injection speed of 5.0 m/s were higher than 2.0 m/s them.

From the temperature distribution in the simulation shown in Figure 10, it was confirmed that the fracture surfaces of samples E and F were a gentle temperature gradient and were less affected due to segregation. In other words, the segregation is greater affected the tensile strength and the elongation than the porosities. Samples G and H were destroyed in fillets. In sample G, the porosities with a diameter of 0.5 mm or more were distributed from the upper left to the lower right similar to sample F. Sample H was a little porosity. It was confirmed that segregation affected the destruction smaller the porosity size and the greater the variability of porosity.



Observation area of microstructure

Fig. 3 -Tensile test specimen

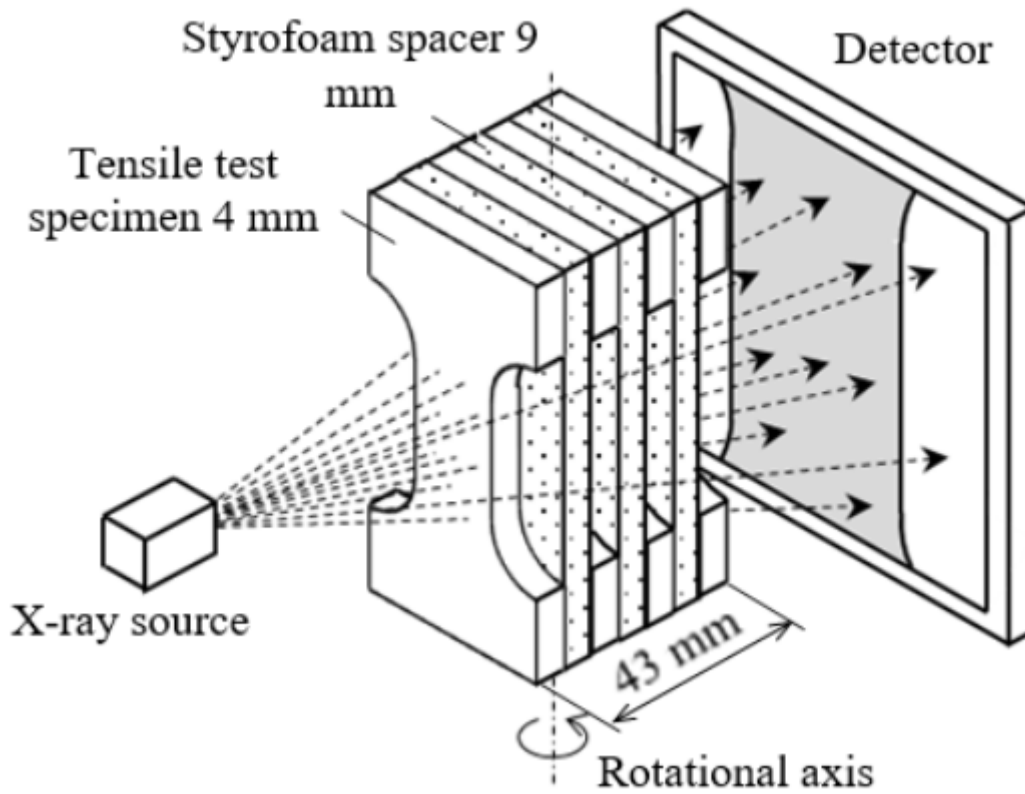


Fig. 4 - X-ray CT set-up

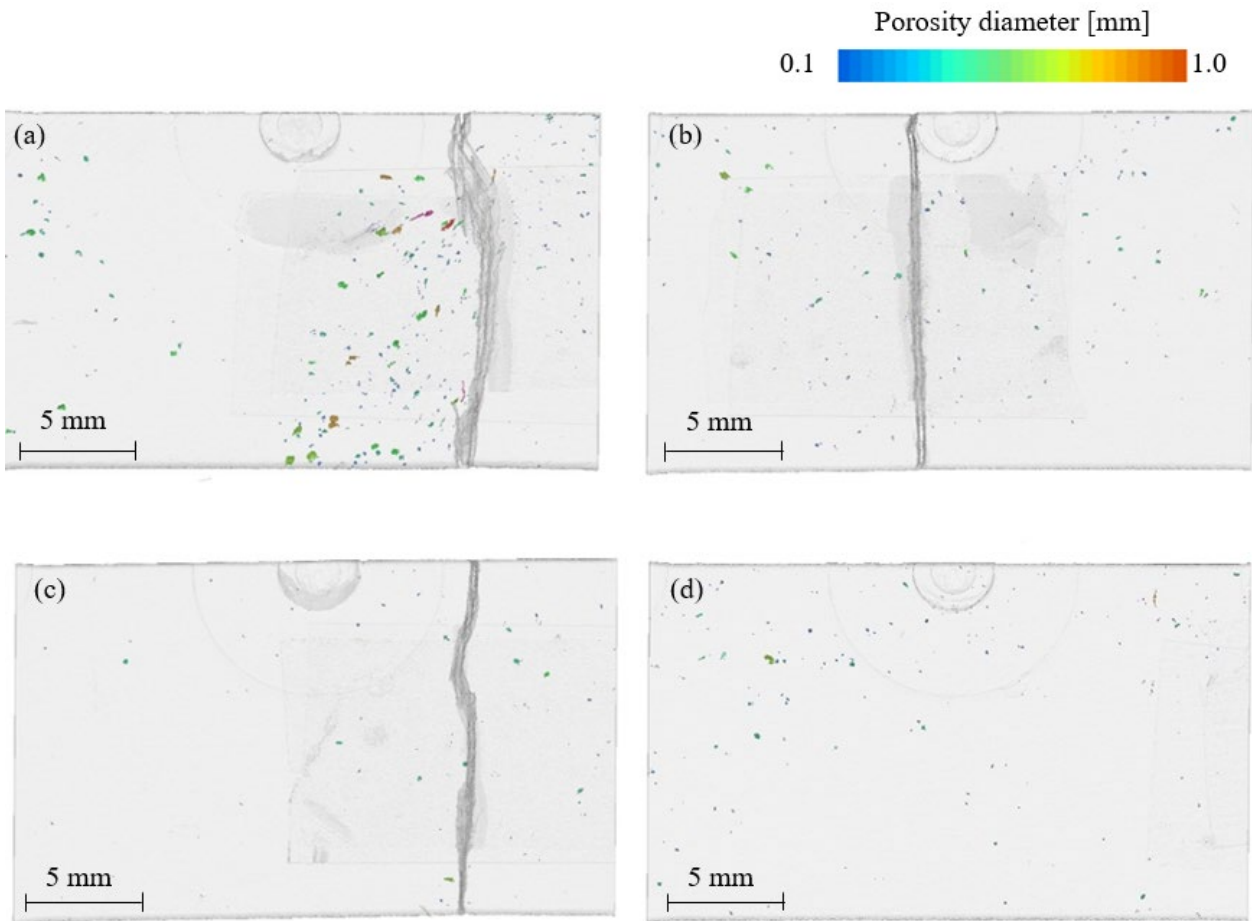


Fig. 5 - X-ray CT images of porosities and destruction types at the gage length sections of tensile tested samples for the plate thickness of 4 mm at the injection speed of 2.0 m/s (a) sample A; (b) sample B; (c) sample C; (d) sample D

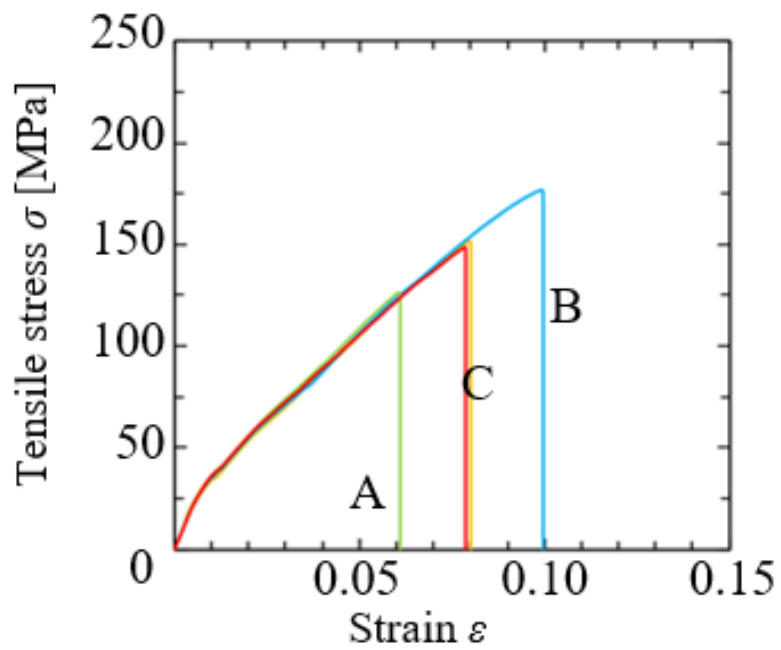


Fig. 6 - Stress-strain curve for the plate thickness of 4 mm at the injection speed of 2.0 m/s

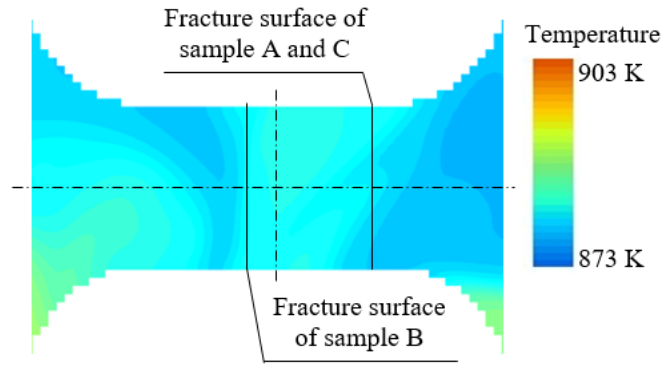


Fig. 7 - Simulation result of temperature map for the plate thickness of 4 mm at the injection speed of 2.0 m/s

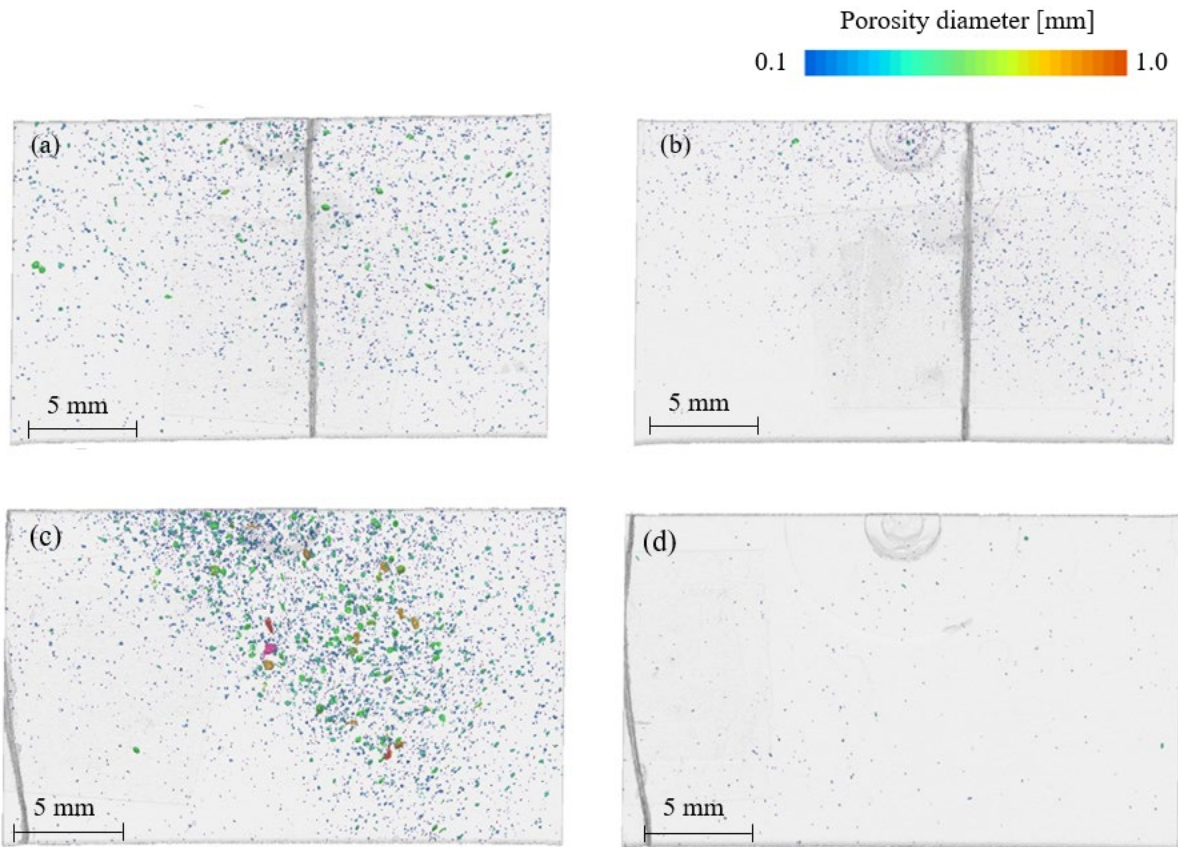


Fig. 8 - X-ray CT images of porosities and destruction types at the gage length sections of tensile tested samples for the plate thickness of 4 mm at the injection speed of 5.0 m/s (a) sample E; (b) sample F; (c) sample G; (d) sample H

3.2 Microstructure and Solidification Speed

Figure 11 shows the surface microstructures for the plate thickness of 4 mm. The dendrite structure was observed at the injection speed of 2.0 m/s. At the injection speed of 5.0 m/s, the eutectic crystals were scattered into clearances of the clumped primary crystal α -Mg. Figure 12 shows the relationship between the eutectic distance and the area rate of the eutectic. The plot shows the mean value and the error bar shows a range of the maximum and minimum variation. The area rate of eutectic was within the range of 40 to 50% regardless of the injection speed. The mean eutectic distances were different results for 10.4 μm on the step side microstructure and 12.0 μm on the other side microstructure in the injection speed of 2.0 m/s, although they were similar results for 8.4 μm and 8.6 μm on each side in the injection speed of 5.0 m/s. It is noticeable to refer to a solidification structure and a cooling speed. In the injection speed of 5.0 m/s, the time of α -Mg coexisting with liquid was shortened, and eutectic phases were formed in the spongy scattered gaps due to disappeared dendrite gaps. The tensile strength increased because the interface between the scattered primary crystals and eutectic systems was narrow. On the other hand, on the flat side with an injection rate of 2.0 m/s, the solid-liquid coexistence time lasted longer than that with the injection rate of 5.0 m/s, and

it grew like a dendrite. A spiderweb-like gap is formed between dendrites, and eutectic crystals are formed in this portion. Since the interface between the primary and eutectic crystals stretched in a spider web shape is wide, the tensile strength decreased. The cooling rate is affected by the increase in thermal resistance as the injection rate increases. Since the heat transfer in the mold in die casting is forced convection, the Nusselt number Nu can be expressed by the function of the Reynolds number Re and the Prandtl number Pr . Here, the Prandtl number is considered to be constant considering that the molten metal is completely fluid. That is, the Nusselt number is represented by a function of only the Reynolds number. The Nusselt number can be expressed by the ratio of the thermal conductivity λ and the heat transfer coefficient α , and if λ is regarded as constant, the Reynolds number and α have a proportional relationship. That is, as the injection rate increased, the amount of heat transferred between the molten metal and the wall surface also increased, resulting in quick freezing and solidification.

The staircase side with an injection speed of 2.0 m/s covers both the flat side and the particle size range with an injection speed of 5.0 m/s. This is considered to be related to the thickness of the temperature boundary layer near the wall surface. When the injection speed is different, the injection speed of 2.0 m/s has a thicker velocity boundary layer and temperature boundary layer and a gentler velocity gradient and temperature gradient near the wall surface than the injection speed of 5.0 m/s. As a result, the molten metal on the flat side with the injection speed of 2.0 m/s was delayed in solidification and dendrite growth became remarkable. Furthermore, on the side of the stairs, the mainstream flowing from the 6 mm thick gate collides at a step between 4 mm and 8 mm, and a new boundary layer is created from there. Since the boundary layer on the staircase side is thinner than that on the flat side, the amount of heat transfer is significantly large. Therefore, the cooling rate on the staircase side was faster than that on the flat side, resulting in a spongy primary crystal structure.

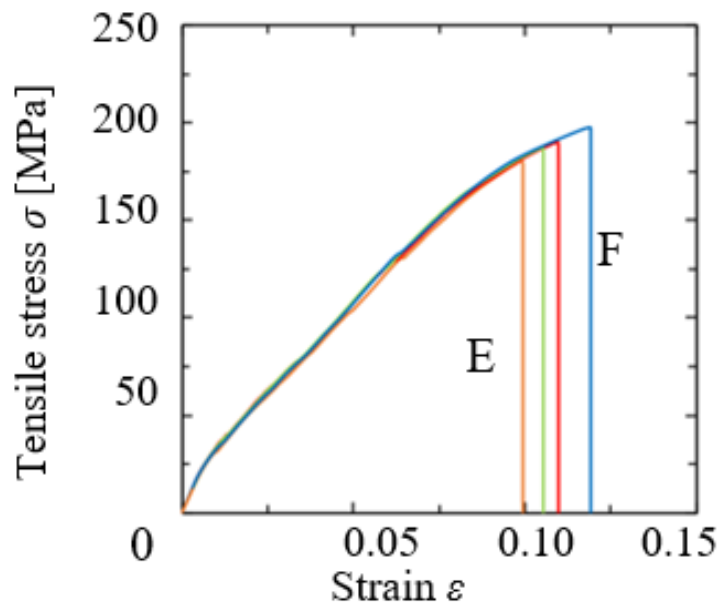


Fig. 9 - Stress-strain curve for the plate thickness of 4 mm at the injection speed of 5.0 m/s

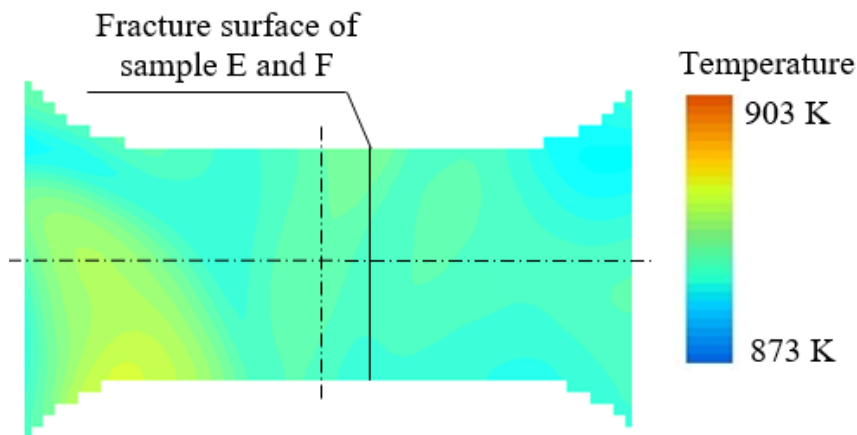


Fig. 10 - Simulation result of temperature map for the plate thickness of 4 mm at the injection speed of 5.0 m/s

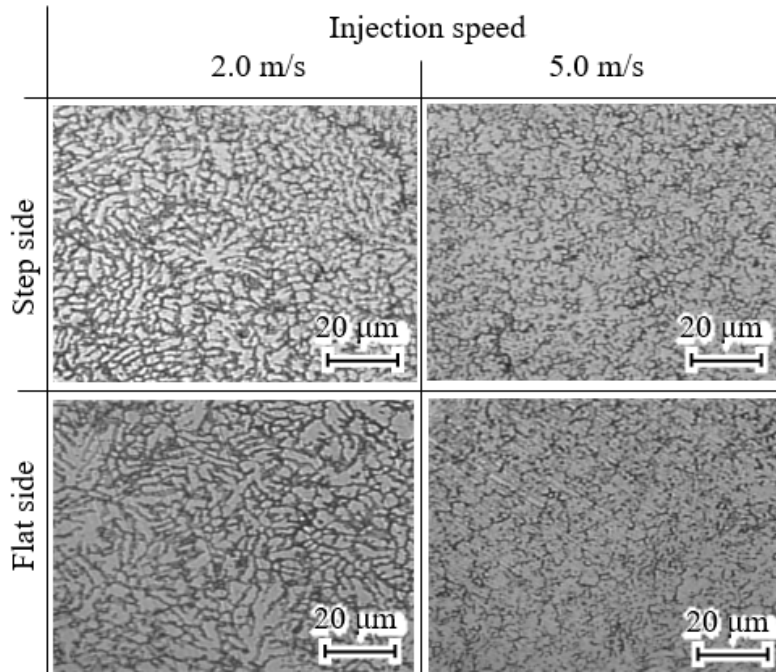


Fig. 11 - Surface microstructure in 4 mm

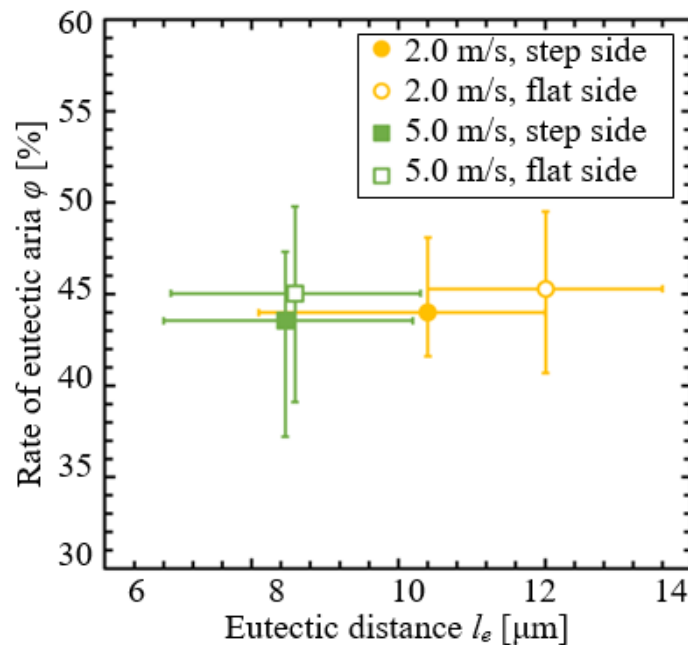


Fig. 12 - Relationship between the eutectic distance l_e and the rate of eutectic area ϕ for the plate thickness of 4 mm

4. Conclusions

In this study, to clarify the unknown physical properties of the Mg-Al-Th-RE alloy, the relationship between casting conditions and internal porosities and the mechanical properties exerted by the solidification structure were investigated. The tensile strength and the elongation at the injection speed of 5.0 m/s were higher than 2.0 m/s them. It was confirmed that the number of porosities affected the tensile strength and the elongation even at the same fracture position. In addition, it was confirmed that segregation affected the destruction smaller the porosity size and the greater the variability of porosity. As the injection rate increased, the amount of heat transferred between the molten metal and the wall surface also increased, resulting in quick freezing and solidification. In the injection speed of 5.0 m/s, the tensile strength increased because the interface between the scattered primary crystals and eutectic systems was narrow. On the other hand, the molten metal on the flat side with the injection speed of 2.0 m/s was delayed in solidification

and dendrite growth became remarkable. The cooling rate on the staircase side was faster than that on the flat side, resulting in a spongy primary crystal structure.

Acknowledgement

This research was partially funded by Kyokuto Die-Casting Co., Ltd., while the X-ray CT measurements conducted in this work were supported by Tokai University Imaging Research Center. This research was also partially supported by Universiti Malaysia Sarawak.

References

- [1] Kuriyama, Y., & Yano, K. (2012). Multi-Subcenters Solution Search Algorithm for CFD Optimization Problems and Its Application to Die Casting. *Mater. Trans.* 53, 367-373
- [2] Ibrahim, M. D., Rahman, M. R. A., Khan, A., Mohamad, M. R., Suffian, M. S. Z. M., Yunus, Y. S., Wong, L. K., & Mohtar, M. Z. (2017). Effect of mold designs on molten metal behavior in high-pressure die casting. *Journal Physic: Conference Series.* 822, 1-6
- [3] Niida, A., & Maeda, Y. (2020). Observation of Air Entrapment during Mold Filling of Die Casting Using Water Model Experiment for Mold Filling Simulation. *Mater. Trans.* 61, 1364-1368
- [4] Gaspar, S., & Pasko, J. (2016). The Research of the Fracture Process and Analysis of the Foundry Errors of Die Castings from Hypoeutectic Silumin. *MM Science Journal.* 2016, 1265-1268
- [5] Gaspar, S., & Pasko, J. (2019). Plunger Pressing Speed-Link the Main Factor Influencing the Mechanical Properties of Die Casting. *MM Science Journal.* 2019, 3490-3493
- [6] Moscovitch, N., Gertsberg, G., Nagar, N., Yehuda, R., Fantetti, N., & Bronfin, B. (2007). Design Guidelines for Components Die Cast in Creep-Resistant Magnesium Alloys MRI153M and MRI230D SAE Technical Paper 2007. 01, 1-8
- [7] Ebel-Wolf, B., Walther, F., & Eifler, D. (2008). Influence of elevated temperatures on the cyclic deformation behavior of the magnesium die-cast alloys AZ91D and MRI230D. *Material Science Engineering.* 486, 634-640
- [8] Mizutani, M., Yoshida, K., Kawabe, N., & Saikawa, S. (2019). Features and Vehicle Application of Heat Resistant Die Cast Magnesium Alloy SEI Technical Review No. 88 (Osaka: Sumitomo Electric Industries, Ltd.) pp 116-121.
- [9] Mondal, A. K., Fechner, D., Kumar, S., Dieringa, H., Maier, P., & Kainer, K. U. (2010). Interrupted creep behavior of Mg alloys developed for powertrain applications. *Material Science Engineering.* 527, 2289- 2296
- [10] Sun, Z., Geng, X., Ren, L., & Hu, H. (2020). Microstructure, Tensile Properties and Fracture Behavior of HPDC Magnesium Alloy AZ91. *International Journal Material Mechanical Manufacturing.* 8, 50-56